# Adsorption Removal of Cationic Dye (Methylene Blue) and Anionic Dye (Congo Red) into Poly(m-aminophenol)/x%$SnO_2$ Nanocomposite (with x = 1, 3, and 10)

**Bouabdellah Daho[1], Abdelkader Dehbi[1,*], Bassaid Salah[1], Ould hamadouche Ikram[1], Zidouri Hadjer[1], Ali Alsalme[2], Giovanna Colucci[3] and Massimo Messori[3]**

[1] *Engineering Physics Laboratory, University of Tiaret, Tiaret, 14000 Algeria.*

[2] *Department of Chemistry, College of Science, King Saud University, Riyadh 11451, Saudi Arabia.*

[3] *Department of Applied Science and Technology (DISAT), Politecnico di Torino, Corso Duca degli Abruzzi 24, 10129 Torino, Italy*

*Corresponding author: *Dehbi Abdelkader, Email:* abddehbi@gmail.com

## Abstract

This study details the synthesis of organic/inorganic hybrid materials by combining the conductive polymer poly(m-aminophenol) (PMAP) with $SnO_2$ metal oxide. The objective is to broaden the polymer's environmental applicability and evaluate its adsorption capabilities, focusing on dyes such as Methylene Blue (MB) and Congo Red (CR). The nanocomposite is meticulously formed through in situ polymerization of m-aminophenol in the presence of $SnO_2$, with varying loading ratios (1%, 3%, 10%). Extensive characterization, including analytical techniques (IR and XRD), confirms the structural integrity of the synthesized materials. X-ray diffraction (XRD) analyses distinctly show the successful combination of $SnO_2$ with the polymer matrix. Adsorption kinetics and isotherm were implemented to understand the adsorption mechanism for both dyes. It was found that PMAP/x%$SnO_2$ nanocomposite materials (with x = 1, 3 and 10) have high adsorption affinity toward MB and low adsorption affinity toward CR. Significantly, the MB removal percentage follows an ascending trend, starting at 85% for pure PMAP and increasing to 89% for PMAP/1%$SnO_2$, to 92% for PMAP/3%$SnO_2$, and peaking at 95% for PMAP/10%$SnO_2$ within 30 minutes. In contrast, CR removal exhibits a lower percentage, with only 54% removal for pure PMAP and a modest increase to 59% for the PMAP/10%$SnO_2$ nanocomposite, representing a 5% improvement. These outcomes lead to the conclusion that PMAP/x%$SnO_2$ nanocomposite materials (with x= 1, 3, and 10) exhibit high adsorption affinity for MB and comparatively lower adsorption affinity for CR. The adsorption of MB and CR on the PMAP and on the PMAP/10%$SnO_2$ nanpcomposite successfully followed the Langmuir adsorption kinetics

model, which showed a better fit for the adsorption of MB and CR. The maximum adsorption capacity ($\boldsymbol{Q_m}$) of MPAP/10%$SnO_2$ for MB was 76.99 mg/g, while for CR it was 39.56 mg/g.

Key words: poly (m-aminophenol), nanocomposites, tin oxide, dyes, adsorption, isotherm

# 1. INTRODUCTION

The formidable challenge in the technological utilization of polyaniline (PANI) arises from its inherent low solubility. The unsubstituted PANI in salt form demonstrates insolubility in common organic solvents [1-6]. However, the landscape changes with substituted PANI derivatives, such as poly(o-toluidine), poly(o-anisidine), poly(aniline-co-o-nitroaniline), and poly(aniline-co-o-anisidine), which exhibit enhanced solubility compared to their unsubstituted counterpart [7–9]. The growing interest in conjugated polyaminoarenes, including PANI and its derivatives, is primarily fueled by their improved solubility and holds immense potential for technological applications in chemical power sources and electrochromic displays [10]. Of particular note, aminophenols stand out as intriguing electrochemical materials. In contrast to aniline and other substituted anilines, aminophenols possess two distinct groups (–$NH_2$ and –OH) susceptible to oxidation. This dual functionality enables them to exhibit electrochemical behavior reminiscent of both anilines [11–13] and phenols [14, 15]. The unique electrochemical properties of aminophenols render them captivating candidates for various applications, making them particularly appealing in the realm of sensor technology.

To address the challenges posed by pollution, various depollution methods have been employed, including precipitation, adsorption on activated carbon and clay, ion exchange, membrane separation, solvent extraction, and more. However, practical experience has revealed that these methods often fall short in effectively addressing the widespread nature of pollution or are associated with prohibitive costs. Physicochemical treatments, for instance, demand significant quantities of oxidizing agents and may result in the formation of undesirable and potentially toxic intermediate by-products.

In response to these limitations, advanced oxidation processes (AOPs), particularly heterogeneous photocatalysis, have emerged as promising solutions for mitigating pollution in aquifer environments. Heterogeneous photocatalysis, a subset of AOPs, has demonstrated the capability to mineralize a wide range of organic compounds. The fundamental principle of photocatalysis relies on the absorption of light radiation by a semiconductor, with energy equal to or exceeding the band gap of the absorbing material ($h\nu \geq Eg$). This energy absorption induces the excitation of an electron, prompting its migration from the valence

band to the conduction band of the semiconductor. Consequently, an electronic deficit or "hole" is created in the valence band, imparting oxidizing-reducing properties to the adsorbed pollutants. The resulting electron/hole charge pairs initiate a direct attack on the pollutants and the formation of hydroxyl radicals, facilitating the initiation of photocatalytic degradation. This process has diverse applications and often leads to the mineralization of pollutants, resulting in their complete elimination and the reduction of toxicity.

In recent years, there has been a substantial surge in research focused on the polymerization of o-, m-, and p-aminophenol [16–20]. The extensive literature on the subject indicates that poly(o-, m-, p-aminophenol) tends to exhibit greater solubility than unsubstituted polyaniline (PANI) in common organic solvents. Notably, m-aminophenol (3-amino phenol) (MAP) follows a polymerization process akin to that of aniline. Typically, the chemical polymerization of MAP is accomplished in acidic solutions, employing oxidizing agents such as ammonium peroxydisulphate (APS) [21–23]. This methodology has proven effective in facilitating the synthesis of polymerized m-aminophenol, paving the way for the exploration of its unique properties and potential applications. The soluble nature of poly(m-aminophenol) positions it as a promising candidate for diverse applications, and the utilization of APS as an oxidant agent adds a layer of versatility to the synthesis process.

In recent times, there has been a burgeoning interest in the development of nanoscale inorganic/polymer hybrid materials, fueled by the vast array of potential applications they offer. These nanocomposite materials have swiftly become the focus of extensive global research, showcasing their versatility and applicability in a myriad of technological domains. Notably, they have demonstrated significant promise in the realm of effective quantum electronic devices, magnetic recording materials, and sensors, contributing to the evolution of cutting-edge technologies [24]. Furthermore, the synergy achieved in nanocomposite materials comprising conducting polymers and oxides has opened up new avenues for applications, extending beyond traditional boundaries. This class of materials has found utility in diverse fields, including drug delivery systems, conductive paints, rechargeable batteries, toners in photocopying, smart windows, and more [25, 26]. The multifaceted nature of these inorganic/polymer hybrid nanocomposites positions them as pivotal contributors to technological advancements across various industries and environmental.

In the scope of this investigation, the synthesis of poly(meta-aminophenol) (PMAP) was achieved through a chemical method utilizing ammonium peroxydisulphate (APS) as the oxidant [27-31]. Concurrently, the development of PMAP/$SnO_2$ composites was undertaken

via a conventional in situ chemical oxidative polymerization process [32-36]. This involved the polymerization of meta-aminophenol (MAP) in the presence of $SnO_2$ particles. The resulting polymer samples underwent comprehensive characterization employing a suite of analytical techniques, including Fourier-transform infrared spectroscopy (FTIR), and x-ray diffraction (XRD). FTIR provided insights into the molecular structure and functional groups present in the synthesized materials. The adsorption mechanism of BM and CR onto the material's surface might arise not solely from electrostatic interactions between BM and CR molecules (anionic dye) and the material, but potentially from hydrogen bonding between BM and CR molecules and PMPA/10%$SnO_2$. This interaction is deemed crucial in driving the adsorption phenomenon.

## 2. MATERIALS AND METHODS

The synthesis of poly(meta-aminophenol) was conducted in an acidic medium using a standard procedure. The monomer, m-aminophenol (m-AP), was initiated by the gradual addition of the oxidizing agent, ammonium peroxydisulphate (APS), and concentrated $H_2SO_4$ served as a dopant. This process took place under continuous stirring at a temperature range of 0-5°C. Maintaining a monomer to oxidizing agent ratio of 1:1, 4.18 units of m-AP were combined with 4.56 units of APS. Following the complete addition of the oxidizing agent, the reaction mixture underwent continuous stirring for 4 hours. Subsequently, the resulting product was filtered and washed with distilled water until the filtrate became colorless. Finally, the polymer was dried and processed into a powdered form, culminating in the successful synthesis of poly(meta-aminophenol).

The tin dioxide nanoparticles were synthesized using the sol–gel method [37]. In a standard procedure, 8.35g of hydrated tin chloride ($SnCl_2.2H_2O$) was dissolved in 100ml of pure ethanol ($C_2H_5OH$). The resulting solution underwent magnetic stirring for 30 minutes in a closed three-necked flask. Subsequently, the solution was continuously refluxed at 80°C for 2 hours to generate the $SnO_2$ sol solution. Prior to the calcination process at 650°C for 1 hour, the sol was dried at 100°C for 30 minutes, resulting in the formation of well-defined tin dioxide nanoparticles. This method ensures the controlled synthesis of $SnO_2$ nanoparticles through precise sol formation and subsequent controlled calcination, providing a reproducible and effective route for their preparation.

The poly(m-aminophenol)/$SnO_2$ nanocomposites were fabricated through an in situ chemical oxidative polymerization process of the m-aminophenol (m-AP) monomer in the presence of

$SnO_2$ particles. Initially, $SnO_2$ particles were dispersed in 50 mL of chloroform under ultrasonic vibrations at room temperature for 10 minutes. Subsequently, m-AP (3.27 g, 10 mmol) was introduced into different weight percentages (1%, 3% and 10% wt) of the $SnO_2$ dispersion in 50 ml of 1N $H_2SO_4$ under vigorous stirring. Concurrently, 10.27 g (15 mmol) of ammonium peroxydisulphate (APS) was dissolved in 50 ml of 1N $H_2SO_4$. The aqueous APS solution was then added drop by drop to the m-AP solution, and the entire mixture was continuously stirred for 30 minutes. The reaction took place in an ice bath for 4 hours. Throughout the process, the color of the mixture transformed from gray to a deep black hue, indicative of the successful polymerization and the formation of poly(m-aminophenol)/$SnO_2$ nanocomposites.

The solubility of PMAP was assessed using various solvents. A 20 mg powder sample of the polymer was introduced into 10 mL of each solvent, including water, chloroform, diethyl ether, and dimethyl sulfoxide (DMSO), and meticulously dispersed. Subsequently, the mixture underwent continuous stirring at room temperature, allowing for the examination and determination of the polymer's solubility in each solvent. This approach provides valuable insights into the polymer's compatibility with different solvents, aiding in the understanding of its potential applications and handling characteristics.

The X-ray diffraction (XRD) patterns for the samples were acquired under ambient conditions utilizing a Philips X-ray powder diffractometer with Cu $K_\alpha$ radiation ($\lambda$ = 1.5406 Å). Scans were conducted at a rate of 2°/min within the angular range of 20–80°. Fourier-transformed infrared (FTIR) spectra were obtained using a Jasco FT/IR-4200 (ATR) spectrometer employing the KBr pellet method.

All adsorption equilibrium experiments of Methylene Blue and Congo Red on PMAP and PMAP/$SnO_2$ composite in water were carried out in batch mode in a double-walled reactor under dark conditions at 25°C for 30 min. Studies were made using suspensions prepared by mixing a 50ml solution of various initial concentrations (10 mg/l) of MB and CR in water at their pH (5.5 and 6.5) and 0.01g of samples (PMAP or PMAP/$SnO_2$). The equilibrium concentrations of MB and CR in the solution were studied after centrifugation by measuring the change in absorption intensity at $\lambda_{max}$ by using a UV-1650PC spectrophotometer.

The Zero Charge Point pH ($pH_{PZC}$) or pH of the point of zero charge corresponds to the pH value for which the net charge of the surface of the adsorbent is zero. The solid addition method was used to determine the zero point charge of the PMAP/10%$SnO_2$ nanocomposite

material adsorbent (0.1 g) was added into each of five beakers containing 50 ml of $KNO_3$ solution (0.01M). The initial pH of the $KNO_3$ solutions was adjusted to pH 2, 5.5, 7, 9 and 11 using KOH (0.1 M) and $HNO_3$ (0.1 M) solutions. After 24 hours of agitation, all beakers were withdrawn from the stirrer and the final pH was measured using a typical pH meter. The intersection point on the curve ($pH_i - pH_f$) versus $pH_i$ was estimated as the pH value of Zero Charge Point.

## 3. Results and discussion

The solubility test showed that PMAP is insoluble in nonpolar solvents, such as chloroform and ether. It is also insoluble in dichloromethane, a polar aprotic solvent. In slightly polars solvents, such as DimethylSulfoxide (DMSO), PMAP exhibits good dispersion. In this case, it is inappropriate to talk about the solubility of the polymer. Indeed, the dissolution of the polymer by a solvent implies that the molecules of the solvent (solvated) surround each molecule (each unit of the monomer for a polymer). Consequently, it is legitimate to speak of dispersion rather than solubility [38]. In polar media, such as water, PMAP does not solubilize but swells slightly. This is probably due to water molecules, which interpose between the PMAP particles and form hydrogen bonds with the OH groups of PMAP [39].

The FTIR spectra of PMAP and nanocomposite PMAP/ x% $SnO_2$ (x=1.3.10%), as depicted in Figure 1, reveal distinctive bands indicative of various molecular vibrations. Notably, the bands in the range of 600 to 810 $cm^{-1}$ can be ascribed to the deformation vibration of the aromatic =C-H bonds. The peak observed at 1050 $cm^{-1}$ is attributed to the stretching vibrations of the C-O-C bonds, a characteristic feature associated with the transformation of precursor materials, including meta-aminophenol, into the polymer PMAP. Furthermore, the vibrational band at 1283 $cm^{-1}$ corresponds to the C-N bond of the aromatic amine, suggesting the establishment of a C-N-C structure within the polymer matrix.

Additionally, the presence of bands spanning from 1500 $cm^{-1}$ to 1585 $cm^{-1}$ signifies vibrations associated with the C=N and C=C double bonds, providing further insights into the structural composition of PMAP. Notably, a broadband extending from 2500 $cm^{-1}$ to 3700 $cm^{-1}$ is observed, indicating the amalgamation of two absorption bands related to the stretching vibrations of –OH, $–NH_2$, and the aromatic groups –CH. This spectral information contributes to a comprehensive understanding of the molecular composition and bonding arrangements present in the synthesized PMAP polymer.

The strong and wide absorption band, located below 800 $cm^{-1}$, is characteristic of the stretching vibration of Sn-O. This band is wider in pure $SnO_2$. The narrowing of this band in the spectra of the PMAP 10%$SnO_2$ nanocomposite material could be attributed to a disorder in the structure of the nanocomposite material, which results from the combination of PMAP with $SnO_2$.

The diffractogram of PMAP and nanocomposite PMAP/ x% $SnO_2$ (x=1.3.10%), as illustrated in Figure 2, exhibits a distinctive pattern characterized by diffuse and broadened lines. This unique diffraction profile is a clear indication of the presence of disordered zones within the polymer structure. The observation of diffuse lines in the diffractogram is a characteristic feature associated with materials that possess an amorphous structure. In the case of poly(m-aminophenol) or PMAP, the amorphous nature is evident from the absence of sharp, well-defined diffraction peaks that would typically be indicative of a crystalline structure. The existence of disordered zones and the overall amorphous nature of PMAP are critical aspects influencing its material properties. Amorphous polymers often exhibit advantageous characteristics, such as enhanced solubility and processability, making them suitable for various applications, including coatings, adhesives, and certain types of sensors. The diffractogram analysis, therefore, provides valuable insights into the structural arrangement of PMAP, guiding our understanding of its potential applications and informing future research directions aimed at optimizing its properties for specific uses.

The identification of the crystalline phases within tin dioxide powder, calcined at 650°C, was conducted across a scanning range from 3° to 80°. Analysis of the diffractogram presented in Figure 2 reveals distinct lines corresponding to the planes (110), (101), (200), (211), (220), (310), and (301). These observations align with the characteristic diffraction pattern of tetragonal tin dioxide, as documented in the JCPDS Powder Diffraction File Card 5-0467. The preferential orientation of these lines along the [111] plane further signifies the crystalline nature of the tin dioxide phase.

Upon examining the X-ray diffractogram of the PMAP/1%$SnO_2$, PMAP/3%$SnO_2$, and PMAP/10%$SnO_2$ nanocomposites, as depicted in Figure 2, three prominent peaks at 25°, 35°, and 53° emerge conspicuously. These peaks align precisely with the characteristic diffraction peaks of $SnO_2$, providing clear evidence for the presence of tin dioxide particles within the PMAP matrix. The discernible peaks at specific angles substantiate the successful

incorporation of $SnO_2$ into the nanocomposite structures, offering valuable insights into the crystalline phases and confirming the effective integration of $SnO_2$ within the PMAP matrix.

Figures 3 and 4 give the results of MB and CR adsorption kinetics on PMAP and on PMAP/x%$SnO_2$ nanocomposite materials (with x = 1, 3 and 10) in water. The fixation ratio, expressed as a percentage, provides a quantitative measure of the effectiveness of dye removal by materials (insert figures).

During the first 5 minutes, the elimination of the MB is very rapid: for example, around 80% of the MB was eliminated for the PMAP/10%$SnO_2$ nanocomposite. Thereafter, MB elimination decreased: approximately 15% of MB were eliminated over the next 25 minutes. It was also observed that the percentage of MB removal increased from 85% for pure PMAP to 89% for PMAP/1%$SnO_2$ nanocomposite, then to 92% for PMAP/3%$SnO_2$ nanocomposite and reached the highest percentage at 95% for PMAP/10%$SnO_2$ nanocomposite for a time of 30 min. Meanwhile, the percentage of CR elimination was the least. Indeed, a removal percentage of only 54% is obtained for pure PMAP, and then it reached a percentage of 59% for the PMAP/10%$SnO_2$ nanocomposite, an increase of 5%. Based on these results, It was concluded that the PMAP/x%$SnO_2$ nanocomposite materials (with x= 1, 3 and 10) have a high adsorption affinity towards the MB and a low adsorption affinity towards the CR.

To obtain an explanation of this phenomenon, adsorption isotherms on pure PMAP and on the PMAP/10%$SnO_2$ nanocomposite were studied. Langmuir isotherm model was used to describe the adsorption of dyes on catalyst materials. $k$ and $Q_m$ were determined by means of non-linear regression fit of the Langmuir equation (Eq. 1):

$$Q_e = \frac{Q_m k C_e}{1 + k C_e} \qquad (1)$$

were $Q_e$ is the adsorbed quantity of dye (mg/g), $C_e$ is the equilibrium concentration of dye (mg/L), $k$ the Langmuir equilibrium constant (L/mg) and $Q_m$ the maximum capacity adsorption of dye on the surface of the catalyst (mg/g).

Figure 5 and 6 show the results of adsorption isotherm of MB and CR on pure PMAP and on the PMAP/10%$SnO_2$ nanocomposite in water. The Langmuir model parameters for MB and CR adsorbed on pure PMAP and on the PMAP/10%$SnO_2$ nanocomposite are summarized in Table 1.

The adsorption results obtained clearly indicate that the maximum adsorption capacity ($\boldsymbol{Q_m}$) of dyes (MB and CR) on the PMAP/10%$SnO_2$ nanocomposite material is higher than that of

pure PMAP. Indeed, the combination of 10% $SnO_2$ oxide with PMAP gives maximum adsorption capacity ($\boldsymbol{Q_m}$) values of 76.99 mg/g and 39.56 mg/g for MB and for CR, respectively. We notice that $\boldsymbol{Q_m}$ for MB is almost double that for CR, this confirms the high adsorption affinity of PMAP/10%$SnO_2$ towards MB. Adsorption in water of MB and CR by PMAP/x%$SnO_2$ nanocomposite materials strongly depends on the pH of the dye solution, the surface charge of the nanocomposite adsorbent and the charge of the dye [40-41]. The pH of the zero point charge ($pH_{PZC}$) for the PMAP/10%$SnO_2$ nanocomposite was determined to be 3.7, as shown in Figure 6. In the presence of water molecules, PMAP/x%$SnO_2$ particles are covered by hydroxide groups. However, if the pH of the medium varies, these OH groups are able to give or tear off proton $H^+$. Figure 8 shows the modification of the PMAP/10%$SnO_2$ charge surface according to the pH. In different pH ranges, there exist electrostatic interaction (attraction or repulsion) between the material surface and the dye molecule. Consequently, this phenomenon can have an effect on adsorption properties. Indeed, the work pH values of the dispersion of the PMAP/10%$SnO_2$ material into 10 ppm MB solution and into 10 ppm CR solution are 5.5 and 6.5, respectively. These pHs are higher than the $pH_{PZC}$, which gives to the surface of the material a negative charge. Consequently, a strong attraction between the MB molecules (cationic dye) and the material, and a weak attraction between the CR molecules (anionic dye) and the material, which leads to a strong adsorption of MB on the surface of the material and a weak adsorption of CR on the surface of the material. The adsorption process of CR on the surface of the material may be due not to the electrostatic interactions between the CR molecules (anionic dye) and the material, but to the hydrogen bonding between the CR molecules and the PMAP/10%$SnO_2$, which also plays a very important role in the adsorption phenomenon [42]

## 4. Conclusion

In conclusion, our study focused on the synthesis and characterization of nanocomposites comprising poly(m-aminophenol) (PMAP) and tin dioxide ($SnO_2$) using an in-situ chemical polymerization technique with varying tin dioxide charge ratios (1%, 3%, 10%). Solubility tests revealed that PMAP exhibits slight solubility in dimethyl sulfoxide (DMSO). X-ray diffraction (XRD) analysis unveiled the amorphous nature of PMAP and the semi-crystalline

structure of PMAP/$SnO_2$ nanocomposites, where distinctive $SnO_2$ peaks confirmed successful tin oxide combination with the polymer matrix.

Furthermore, the performance of PMAP/x%$SnO_2$ nanocomposite materials in adsorbing two different dyes (cationic and anionic), namely Methylene Blue (MB) and Congo Red (CR) in water. The study found that these nanocomposite materials exhibit a high adsorption affinity for MB and a low affinity for CR. Specifically, the removal efficiency of MB increases as the concentration of $SnO_2$ in the nanocomposite rises. The removal percentage for MB starts at 85% for pure PMAP and gradually increases to 95% for PMAP/10%$SnO_2$ within a 30-minutes timeframe. On the other hand, the removal efficiency for CR is lower, with only 54% for pure PMAP and a modest improvement to 59% for PMAP/10%$SnO_2$, representing a 5% increase. This information suggests that the nanocomposite materials are particularly effective in removing MB, with the highest efficiency observed in the presence of 10% $SnO_2$, while the removal of CR shows a comparatively smaller enhancement. The adsorption isotherm data of MB and CR dyes onto the PMAP/10%$SnO_2$ is best fitted by the Langmuir model. A combination of 10% $SnO_2$ oxide with PMAP gives maximum adsorption capacity ($\boldsymbol{Q_m}$) of 76.99 mg/g for MB and 39.56 mg/g for CR.

These findings underscore the potential utility of PMAP and PMAP/$SnO_2$ nanocomposites in applications involving dye removal, with the nanocomposite demonstrating enhanced performance. The successful combination of tin dioxide with the polymer matrix opens avenues for exploring these materials in diverse fields, benefiting from their unique optical, structural, and adsorptive properties. The comprehensive characterization and promising results presented in this study pave the way for further exploration and optimization of these nanocomposites for practical applications in environmental and materials science.

## Acknowledgment

The authors would like to acknowledge the Researchers Supporting Project (RSP-2024R78), King Saud University, Riyadh, Saudi Arabia.

### Statements and Declarations:

**Compliance with ethical standards**

**Conflict of interest:** They have no conflict of interest

### Funding

No funding

# References

[1] Sharma AL, Saxena V, Annapoorni S, Malhotra BD (2001) Synthesis and characterization of a copolymer: poly(anilineco-fluoroaniline), J. Appl. Polym. Sci. 81:1460–1466.

[2] Herrasti P, Recio FJ, Ocón P, Fatás E (2005) Effect of the polymer layers and bilayers on the corrosion behaviour of mild steel: comparison with polymers containing Zn microparticles, Prog. Org. Coat 54:285–291.

[3] Ivanov S, Mokreva P, Tsakova V, Terlemezyan L (2003) Electrochemical and surface structural characterization of chemically and electrochemically synthesized polyaniline coating, Thin Solid Films 441:44–49.

[4] Jeevananda T, Siddaramaiah, Seetharamu S, Saravanan S, D'Souza L (2004) Synthesis and characterization of poly(anilineco- acrylonitrile) using organic benzoyl peroxide by inverted emulsion method, Synth. Met. 140:247–260.

[5] Borole DD, Kapadi UR, Mahulikar PP, Hundiwale DG (2009) Influence of TiO2 and SiO2 on electrochemical, optical and electrical conductivity of polyaniline, poly(o-toluidine) and their co-polymer, Des. Mon. Polym 12:523–532.

[6] Özdemir C, Kaplan Can H, Çolak N, Güner A (2006) Synthesis, characterization, and comparison of self-doped, doped, and undoped forms of polyaniline, poly(o-anisidine), and poly [aniline-co-(o-anisidine)], J. Appl. Polym. Sci 99: 2182–2192.

[7] Gui Li X, Xia Wang L, Rong Huang M, Quing Lu Y, Fang Zhu M, Menner A, Springer J (2001) Synthesis and characterization of pyrrole and anisidine copolymers, Polymer. 42:6095–6103.

[8] Roy BC, Gupta MD, Bhoumik L, Ray JK (2002) Spectroscopic investigation of water-soluble polyaniline copolymers, Synth. Met 130:27–33.

[9] Yalçınkaya S, Çolak N (2012) Synthesis and characterization of poly(Aniline-co-o-Aminoaniline), Des. Monomers Polym 15:147–157.

[10] Konopelnyk OI, Aksimentyeva OI, Tsizh BR, Chokhan MI (2007) Physical and technological properties of the sensor materials based on conjugated polyaminoarenes, Phys. Chem. Solid State 8:786–90.

[11] Yang H, Bard AJ (1992) the application of fast scan cyclic voltammetry. Mechanistic study of the initial stage of electropolymerization of aniline in aqueous solutions, J. Electroanal. Chem 339(1-2): 423-449.

[12] Yamada K, Teshima K, Kobayashi N, Hirohashi R (1995) Electropolymerization of aniline derivatives in non-aqueous solution without a proton donor J. Electroanal. Chem 394(1-2): 71-79.

[13] Chiang J, MacDiarmid AG (1986) Polyaniline': Protonic acid doping of the emeraldine form to the metallic regime, Synth. Met., 1986, 13(1-3): 193-205.

[14] Gattrell M, Kirk DW (1992) A Fourier Transform Infrared Spectroscopy Study of the Passive Film Produced during Aqueous Acidic Phenol Electro□oxidation, J. Electrochem. Soc 139 (10): 2736-2744.

[15] Lapuente R, Cases F, Garces P, Morallon E, Vazquez JL 1998 A voltammetric and FTIR–ATR study of the electropolymerization of phenol on platinum electrodes in carbonate medium: Influence of sulfide, J. Electroanal. Chem. 451(1-2): 163-171.

[16] Ivanov VD, Zhuzhel'skii DV, Malev VV (2008) Comparison of properties of aniline and o-aminophenol polymers obtained using hydrogen peroxide, Russ. J. Electrochem 44:1204–1211.

[17] Bereket G, Duran B (2009) Anticorrosive properties of electrosynthesized poly(m-aminophenol) on copper from aqueous phenylphosphonic acid solution, Prog. Org. Coat. 64:57–66.

[18] Kar P, Pradhan NC, Adhikari B (2008) A novel route for the synthesis of processable conducting poly(m-aminophenol), Mater. Chem. Phys 111:59–64.

[19] Kar P, Pradhan NC, Adhikari B (2010) Induced doping by sodium ion in poly(m-aminophenol) through the functional groups, Synth. Met, 160:1524–1529.

[20] Kong Y, Zhou Y, Shan X, Jiang Y, Yao C (2011) Electropolymerization of m-aminophenol on expanded graphite and its electrochemical properties, Synth. Met 161: 2301–2305.

[21] Zhang J, Shan D, Mu SA (2007) promising copolymer of aniline and m-aminophenol: chemical preparation, novel electric propertis and characterization, Polymer 48: 1269–1275.

[22] Kar P, Pradhan NC, Adhikari B (2010) Effect on structure, processability, and conductivity of poly(m-aminophenol) of the initial acidity/basicity of the polymerization medium, J. Macromol. Sci. Part B 49: 669–679.

[23] Kar P, Behera AK, Adhikari B, Pradhan NC (2010) Optimization for the chemical synthesis of conducting poly (m-aminophenol) in HCl using ammonium persulfate. High Perform, Polym 22: 428–441.

[24] Anderson A, Hunderi O, Granqvist (1980) Nickel pigmented anodic aluminum oxide for selective absorption of solar energy, J. Appl. Phys 51(1): 754- 764

[25] Jarjayes O, Fries H, Bidan G (1995) New nanocomposites of polypyrrole including γ-Fe2O3 particles: electrical and magnetic characterizations, Synthetic69 (1-3): 343-344

[26] Butter worth MD, Corradi R, Johal J, Lascelles SF, Maeda S, and Armes SP (1995) Zeta Potential Measurements on Conducting Polymer-Inorganic Oxide Nanocomposite Particles, J Colloid Interface sci. 174(2): 510-517.

[27] Baleh H, Bouazza A, Benhaoua C, Bassaid S, Dehbi, A, Belfedal A (2021) The structure and Electrical Properties of New Poly(benzaldehyde-co-thiophene)/ SnO2 Composites, Polym. Sci. - A, 63(6): 872-878.

[28] Daho B, Fontanesi C, Messori M, Dehbi A, Belfedal.A (2019) Synthesis and Characterization of Semiconductor Polymer Doped with FeCl3 and I2, Semicond 53(12): 1656-1664.

[29] Bassaid S, Benhaoua C, Taleb M, Sahli M, Dehbi A (2021) Physical and chemical properties of composites based on polythiophene and titanium dioxide nanoparticles for photocatalysis, Polymer Science, Series B 63 (3): 291-303.

[30] Baleh H, Dehbi A, Bassaid S, Belfedal A, Alsalme A, Messori M (2023) Synthesis and characterization of composites of poly(benzaldehyde-co-thiophene)/ TiO2, Journal of Polymer Research 30 (7): 285.

[31] Bouazza A, Bassaid S, Dehbi A, Guarnaccio A, D'Auria M (2023) Synthesis and characterization of TiO2–x% curcumin nanocomposites (with x= 3, 5, and 10): application to the photocatalytic degradation of methylene blue, Reaction Kinetics, Mechanisms and Catalysis 136: 1589-1605.

[32] Bouazza A, Bassaid S, Dehbi A, Hadj-Zoubir N, Alsalme A, Robert D (2023) Use of TiO2/curcumin nanocomposite material deposited on a cellulosic film for methylene blue

photocatalytic degradation under UV light Reaction Kinetics, Mechanisms and Catalysis, 136: 1625–1641.

[33] Bekri I, Gherras H, Dehbi A, Belfdal A (2023)Preparation and Characterization of New Soluble and Thermally Stable Polyazomethine by Polycondensation of Thiophene-2,5-dicarboxaldehyde and Ortho-tolidine for Optoelectronics, Polym. Sci. Ser. B, 65: 487–495

[34] Laoufi, M., Yahiaoui, A., Hachemaoui, A. Gherras H, Dehbi A (2022) Synthesis and characterization of PPDMB poly (pyrrole-co-3,5-dimethoxybenzaldehyde) and PPMB poly (pyrrole-co-2-methoxybenzaldehyde): a new copolymer for solar cells, Colloid Polym Sci 300(10): 1139–1154.

[35] Aris FZ, Hachemaouia, A., Yahiaoui, A. Dehbi A (2022) Synthesis, Characterization, and Microbial Degradation Behavior of Hydrogel Based on Poly(ε-caprolactone) and Methacrylic Anhydride, Polym. Sci. Ser. B 64: 417–428.

[36] Mouacher L, Yahiaoui A, Hachemaoui A, Dehbi A, Benkouider AM (2021) Synthesis and Characterization of Conducting Poly(2-aminothiazole)/Modified-Clay Nanocomposites, Polym. Sci. Ser. B 63: 314–321.

[37] Madzlan AN, Saad SA, Wan R, Wan B (2013) Size-controlled synthesis of SnO2 nanoparticles by sol–gel method, Materials Letters 91: 31–34.

[38] B. Wessling, "Handbook of nanostructured Materials and Nanotechnology", E. Nalwa, ed., Academic press (1999), Vol. 5.

[39] B. Bai, L. Li, Y. Liu, H. L. Zhonguo Wang and C. You, Preformed Particle gel for conformance Control: Factors Affecting its Properties and Applications, . SPE Res Eval & Eng. (2007) 10(04):415–422

[40] Nazeeha S. AlkayalAlkabal NS (2022) Fabrication of Cross-Linked PMMA/SnO2 Nanocomposites for Highly Efficient Removal of Chromium (III) from Wastewater. Polymers, 14(10), 2101.

[41] Siddiqui SI, Zohra F, Chaudhry SA (2019) Nigella sativa seed based nanohybrid composite-Fe2O3–SnO2/BC: A novel material for enhanced adsorptive removal of methylene blue from water. Environmental Research, 178, 108667.

[42] Liu Q, Liu Y, Zhang Z, Wang X, Shen J (2020) Adsorption of cationic dyes from aqueous solution using hydrophilic silica aerogel via ambient pressure drying. Chin. J. Chem. Eng 28: 2467–2473.

**Table 1 :** Langmuir adsorption isotherm parameters of MB and CR on pure PMAP and on the PMAP/10%$SnO_2$ nanocomposite

| | **PMAP** | | **PMAP/10%$SnO_2$** | |
|---|---|---|---|---|
| | MB | CR | MB | CR |
| $Q_m$ *(mg/g)* | 55.1022 | 30.0345 | 76.9871 | 39.5621 |
| ***k (L/mg)*** | 0.3198 ± 0.0080 | 0.3512 ± 0.0019 | 0.2271 ± 0.0020 | 0.4211 ± 0.0045 |
| $R^2$ | 0.9997 | 0.9986 | 0.9999 | 0.9999 |

Figure 1: Characteristic FT-IR peaks about PMAP and PMAP/$SnO_2$ with different ration (1% $SnO_2$, 3% $SnO_2$ and 10% $SnO_2$)

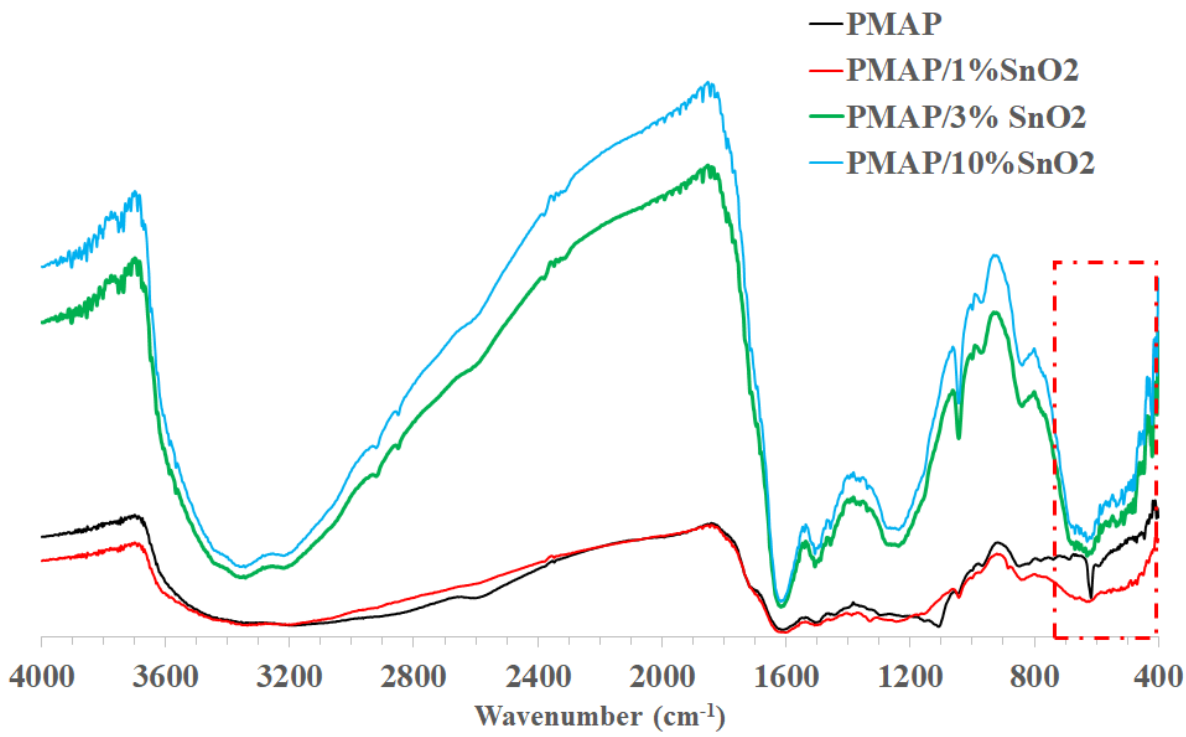

Figure 2: X-Ray diffraction patterns of pure PMAP powder, $SnO_2$ powder and nanocomposites PMAP/$SnO_2$ with different ration (1% $SnO_2$, 3% $SnO_2$ and 10% $SnO_2$)

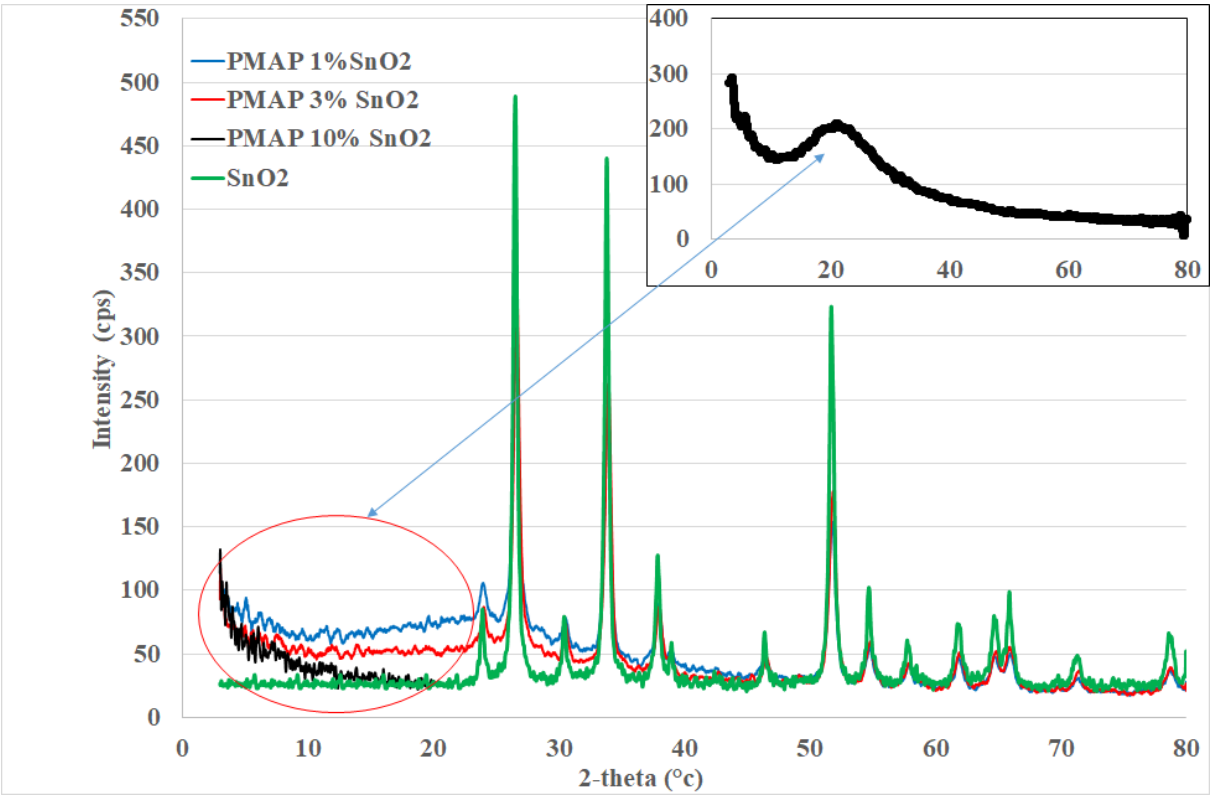

Figure 3 : Kinetics of MB removal by adsorption in water ([MB]) = 10 mg/l) in presence of PMAP and PMAP/x%$SnO_2$ nanocomposites materials (with x = 1, 3 and 10) at pH = 5.5 and T = 25°C.

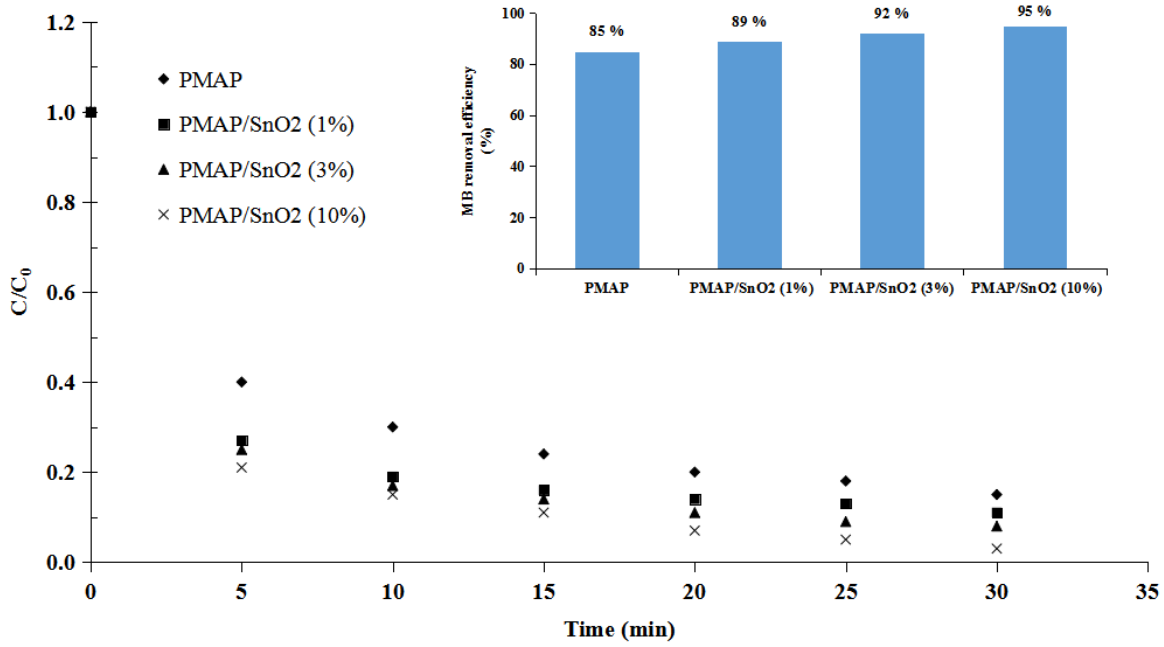

Figure 4: Kinetics of CR removal by adsorption in water ([CR]) = 10 mg/l) in presence of PMAP and PMAP/x%$SnO_2$ nanocomposites materials (with x = 1, 3 and 10) at pH = 6.5 and T = 25°C.

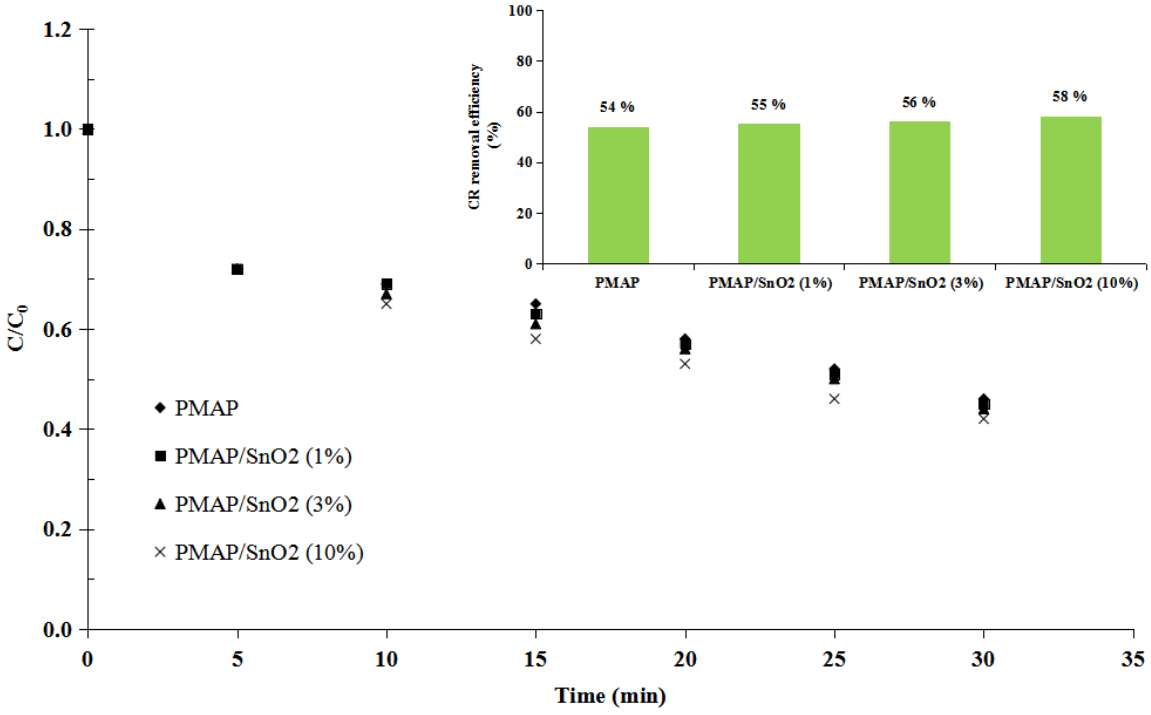

Figure 5: Adsorption isotherm of MB on pure PMAP and on the PMAP/10%$SnO_2$ nanocomposite in water

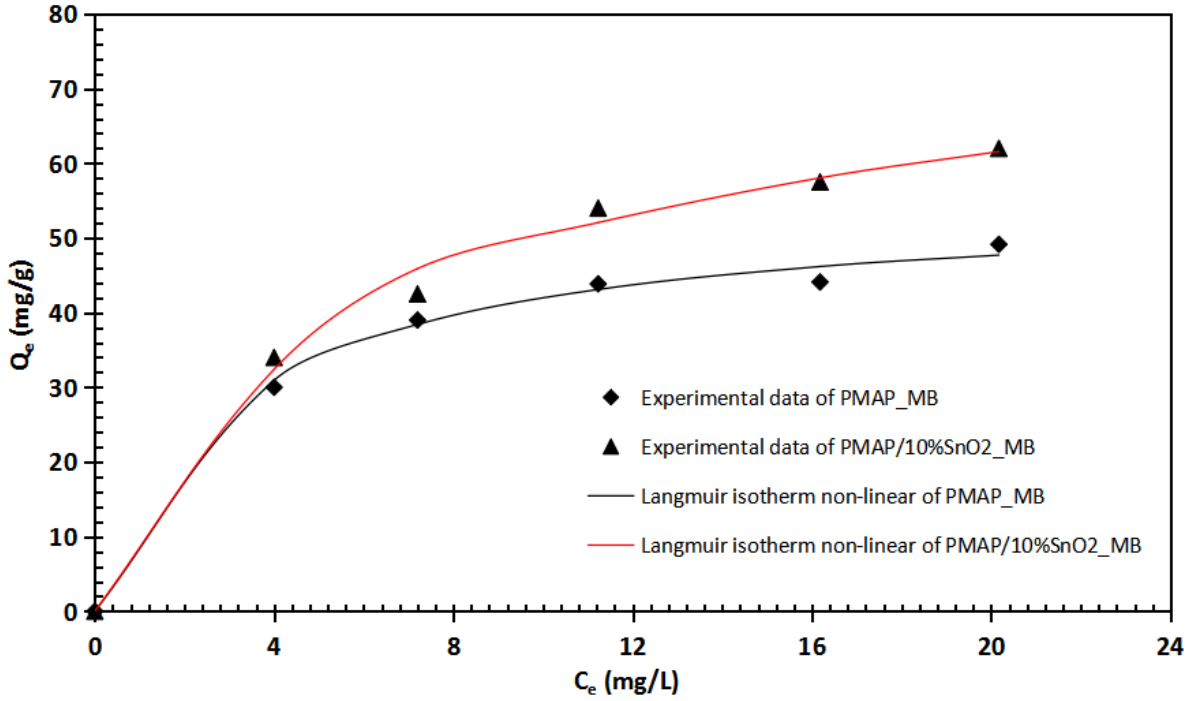

Figure 6: Adsorption isotherm of CR on pure PMAP and on the PMAP/10%$SnO_2$ nanocomposite in water

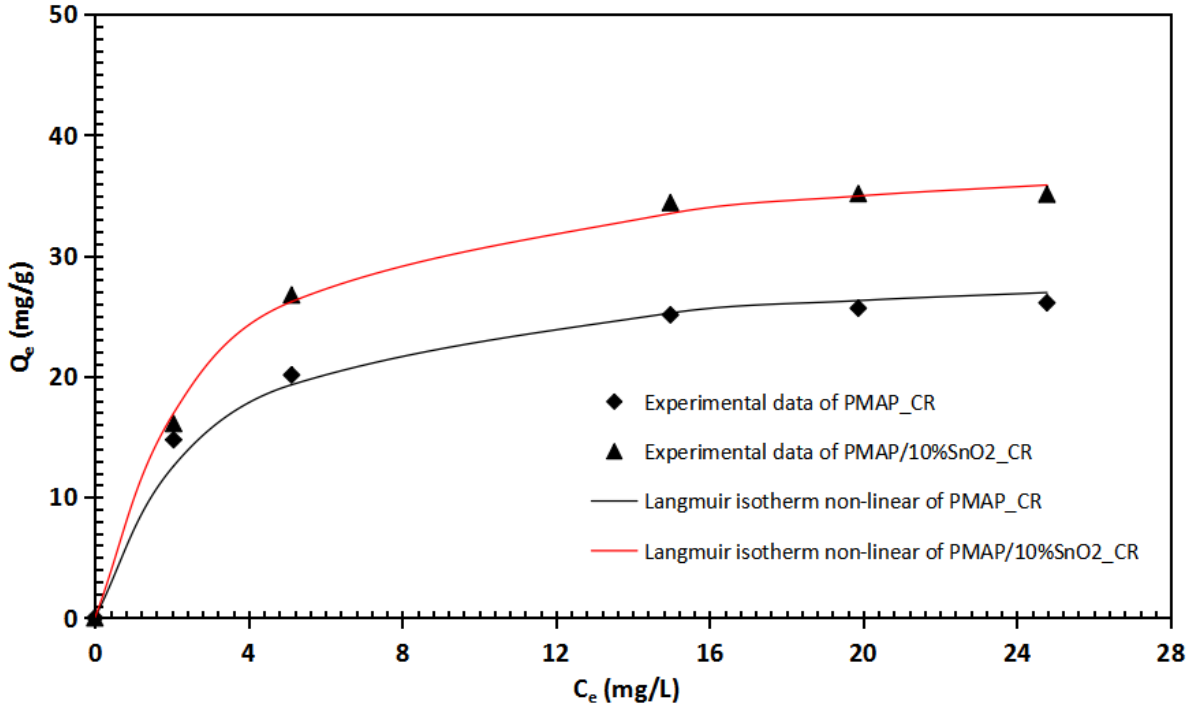

Figure 7: The Zero Point Charge of PMAP/10%$SnO_2$

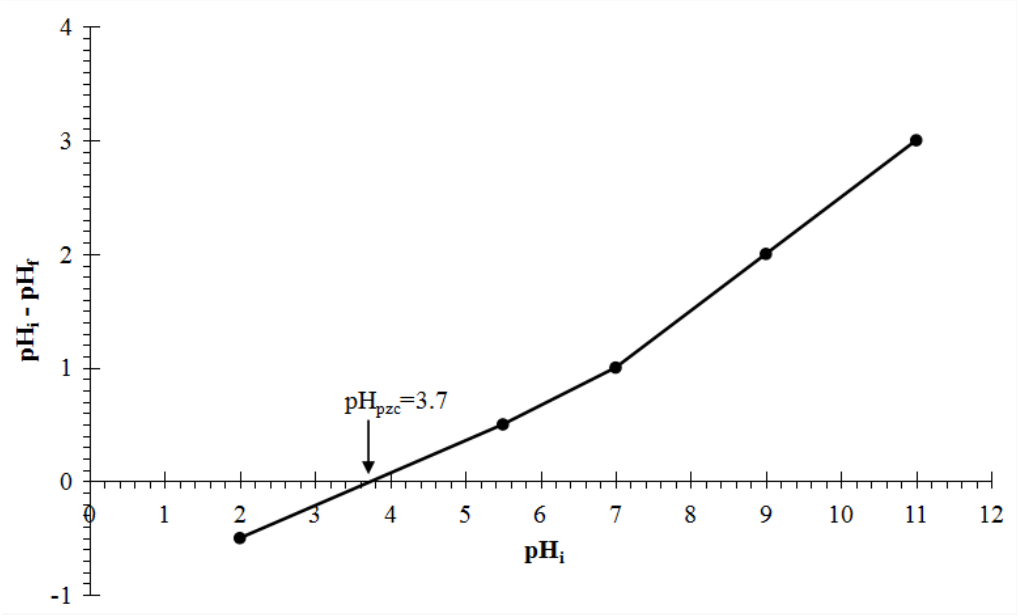

Figure 8: Modification charge of surface of PMAP/10%$SnO_2$ according the pH in different pH ranges

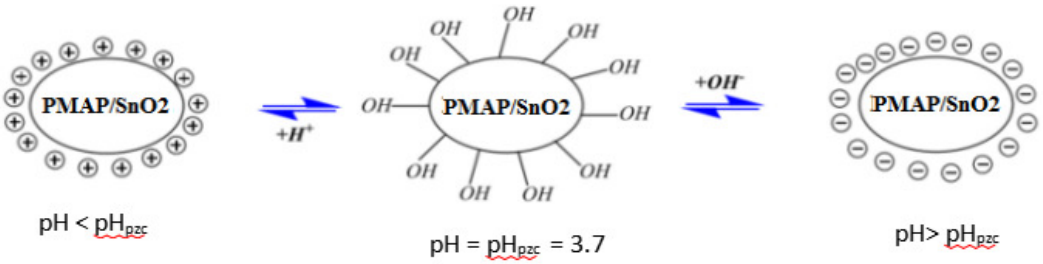


pH < $pH_{pzc}$ pH = $pH_{pzc}$ = 3.7 pH> $pH_{pzc}$